Energetics of oxygen-induced faceting on Cu(115)

D. A. Walko* and I. K. Robinson
Department of Physics, University of Illinois at Urbana-Champaign, 1110 W. Green St., Urbana, Illinois 61801
(Received 01 June 2000; revised manuscript received 30 March 2001; published 5 July 2001)

We have used surface x-ray diffraction to observe the oxygen-induced faceting of the Cu(115) surface in real time. We find that the surface morphological evolution is driven by the formation of O/Cu(104) facets: O exposure induces spinodal decomposition of the (115) surface into (104) and (014) facets, which form spontaneously, and also stepped facets, whose orientation gradually changes from (115) to (113) as the (104) facets grow. We identify three temperature regimes that have qualitatively different faceting processes, allowing us to determine the temperature-dependent equilibrium crystal shape for part of the O/Cu system. Semiquantitative explanations are given in terms of the Wulff construction. During the faceting process, the time evolution follows a slow dynamic scaling, consistent with either a logarithmic or power-law behavior, driven by the rate of incorporation of O onto the surface.

DOI: 10.1103/PhysRevB.64.045412 PACS number(s): 68.35.Bs, 05.70.Np, 61.10.−i, 68.43.Mn

I. INTRODUCTION

Atomic adsorption at surfaces is an important yet incompletely understood process, particularly in cases where adsorption induces a major rearrangement of the surface structure. Changes in morphology can drastically affect many properties of a surface, especially in areas such as catalysis[1–6] and corrosion.[7,8] One of the most dramatic changes a surface can undergo is adsorbate-induced faceting, the breaking up of a surface into facets of differing orientations under the influence of foreign adsorbates; the present work investigates the faceting of a high-Miller-index metal surface due to oxygen adsorption. Low-symmetry, high-index surfaces provide a controlled starting surface (routinely characterized by traditional surface-science techniques) with many potential adsorption sites (steps and/or kinks) from which the effects of adsorption can be generalized to more technologically relevant materials (e.g., polycrystalline surfaces[9] or nanoparticles[10,11]).

While thermal faceting is generally a complex, multistep process,[12] adsorbate-induced faceting[13–15] is further complicated by adsorption kinetics[16,2] and, if applicable, molecular dissociation[17] or other chemical reactions.[18] Once facet nucleation has begun, surface diffusion[19] can become the dominant process in facet growth and coarsening; significant mass transfer is involved in the growth of facets that may be hundreds of Å across. While the surface is, ultimately, driven towards a new equilibrium configuration,[20] the kinetics of adsorption or diffusion can severely affect the surface's final morphology, as can variations in the stability of various orientations.

Previously,[21] we reported the crystallographic structure of facets formed by exposing Cu(115) to O; here we describe the formation of those facets, which we have observed in real time with surface x-ray diffraction. Three stable facets are formed by O adsorption on Cu(115): O/Cu(104), O/Cu(014), and O/Cu(113)(3×1), with the (104) and (014) facets being crystallographically equivalent. We find that a sufficient O_2 exposure induces spinodal decomposition of the surface, which proceeds with a strong temperature dependence. The temperature dependence of the faceting process reflects changes in the relative stability of various facet orientations, and allows us to propose Wulff plots for O-covered Cu facets in the vicinity of (115). The time evolution of the faceting process shows a monotonic, slow growth mode that reflects the slowly increasing stability of the O/Cu(104) facets.

Several metal surfaces have been observed, under the appropriate conditions, to facet upon oxygen adsorption, including many copper surfaces.[22–33] The case of O/Cu(115) is relatively complex, since two well defined but inequivalent types of facets result. In contrast are the cases of O-induced faceting of W(100), W(112), and W(111), since, for sufficiently high O coverage, only O/W{110} facets are formed.[34] As another example, only one smooth surface is formed when O was observed to cause faceting of miscut Ag(110): the surface transformed to regions of smooth O/Ag(110) and heavily stepped regions without a well-defined orientation.[35]

The structures of many faceting systems have been investigated with a variety of surface probes, including low-energy electron diffraction (LEED),[34,36,2] scanning probe microscopies [scanning tunneling microscopy (STM) (Refs. 35,37–39) and atomic force microscopy (Refs. 40–42)], low-energy electron microscopy,[43,44] helium-beam scattering,[45] transmission electron microscopy,[37,8] field ion microscopy,[46–48] reflection electron microscopy,[49] optical microscopy,[50] and optical interferometry.[51] Recently, x-ray scattering methods have been applied to study the thermal faceting of various miscut surfaces, including Cu(110),[52] Ni(111),[53] Pt(001),[54] ice I_h (100),[55] Pt(111),[56] Au(111),[57] Au(001),[58] and Si(113).[59–61] In heteroepitaxial systems, x rays have been used to study the formation of facets on ''hut clusters,'' including {105} facets of Ge/Si(001) (Ref. 62) and {103} facets of In/Ge(001) (Ref. 63), as well as residual strain in Ge pyramids grown on Si(111).[64] In the metal-on-metal systems Cu/Ni(001) (Ref. 65) and Co/Pt(110),[66] x-ray diffraction found that fcc crystallites grow with {111} facets.

II. BACKGROUND: WULFF PLOT AND EQUILIBRIUM CRYSTAL SHAPE

Before moving to a description of the experiment, we very briefly review the theory of equilibrium crystal shapes,

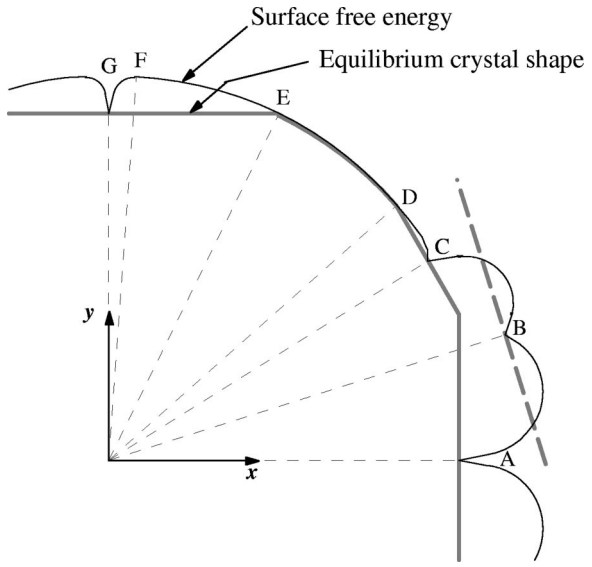

FIG. 1. Sample Wulff construction, showing the surface-free energy vs orientation (outer, thinner line) and the resulting equilibrium crystal shape (inner, thicker line). Dashed lines are radii from the origin to the surface free energy. The effects at orientations *A* through *G* are discussed in the text.

or equivalently, the stability of various surface orientations. The equilibrium shape of a crystal is given by the Wulff construction, i.e., the dependence of surface free energy on orientation.[67] To construct a Wulff plot, radii from the origin are drawn to every point on a polar plot of surface free energy vs orientation. Planes perpendicular to the radii are drawn tangent to the surface free energy plot, with the minimum interior volume representing the equilibrium crystal shape. Mathematically, this is equivalent to a two-dimensional Legendre transformation.[12] Figure 1 provides a two-dimensional example that illustrates important effects found in the O/Cu system as described below.

A cusp (i.e., a local minimum with a diverging derivative) in the Wulff plot denotes a locally stable facet. A locally stable orientation has a lower free energy than immediately adjacent orientations; this is the case for orientations *A*, *B*, *C*, and *G* in Fig. 1. However, another nearby orientation may have such a deep cusp that a facet of the latter orientation is preferred to the former. In the example of Fig. 1, the cusps at orientations *A* and *C* overwhelm the cusp at *B*, so orientation *B* is only a metastable orientation that will not be found on the equilibrium crystal. Surface roughening may occur for a range of orientations that have approximately equal (and locally minimal) free energies;[12] this is the case for orientations *D* to *E* in Fig. 1. No orientations in this range are energetically preferred, and the surface is, statistically, rough.[12] Note, however, that although orientations *D* to *F* have equal free energies, orientations *E* to *F* do not appear as part of the equilibrium crystal shape due to the cusp at *G*. Adsorbates and reconstructions may alter the anisotropy of the surface free energy sufficiently to affect the equilibrium crystal shape,[68,69] perhaps changing relative facet areas or driving some orientations unstable. If adsorption leads to a deep cusp at a given orientation, then a nearby, less stable surface may facet to the more stable orientation if the decrease in surface energy offsets the increase in surface area.

It has long been known[70] that the equilibrium shape of a crystal can be discussed in the language of phase transitions of binary alloys. That is, orientations that appear on the Wulff plot are stable phases. The edges that separate facets are phase boundaries, which can be classified as first-order transitions (in the case of sharp edges) or second-order transitions (for rounded edges).[12] Orientations that do not appear on the Wulff plot (e.g., orientation *B* in Fig. 1) are unstable phases; the faceting of such a surface into stable orientations is thermodynamically favorable[71] and is a case of spinodal decomposition.[72,70,12,73] Several theoretical studies have focused on the stability of various orientations at zero and finite temperature.[15,74–77] Other theoretical work has focused on the late-time evolution of the typical facet length scale $L(t)$, almost always by assuming that the rate-limiting step is the speed of mass transfer as the facets grow. These studies typically find either power-law behavior

$$L(t) \sim t^{\phi} \tag{1}$$

or logarithmic behavior

$$L(t) \sim \ln(t). \tag{2}$$

The choice between these forms (and also the value of the exponent ϕ) depends sensitively on the dimension of the system and the mode of mass transfer. The early work of Mullins[78,79] derived power-law behavior with $\phi = \frac{1}{2}$, $\frac{1}{3}$, or $\frac{1}{4}$ for mass transport in two dimensions by evaporation/condensation, volume diffusion, and surface diffusion, respectively. However, these values are much higher than have typically been observed in experiments[59,42] and some simulations.[80–82] Attempting to explain the slower than expected coarsening rates, Papoular[19] proposed $\phi = \frac{1}{6}$ when kink-antikink reorganization time is the limiting factor in mass transport, while Song *et al.*[60] argued that $\phi = \frac{1}{6}$ when growth proceeds by thermal collisions of step bunches. By working in the continuum limit, Stewart and Goldenfeld[73] found that non-negligible surface stress could destroy any dynamic scaling, while Liu and Metiu[81] derived logarithmic scaling in the case of quasi-one-dimensional surface diffusion. On the other hand, Shore and Bukman[83] argued that coarse-grained models neglect dynamics on the scale of individual steps, which are too important to ignore on vicinal surfaces. Barriers then depend on (grow with) the length scale, which again results in logarithmic scaling.[83] Jeong and Weeks[84] also studied step-step interactions on vicinal surfaces, finding that flat reconstructed terraces grow very fast (in fact, linear in time) along the step direction, but with $\phi = \frac{1}{2}$ or $\frac{1}{4}$ perpendicular to the steps (for global or local mass transport, respectively). Vlachos *et al.*[82] used Monte Carlo simulations to study faceting under equilibrium conditions, finding that the exponent ϕ could vary with temperature, orientation, and material.[82]

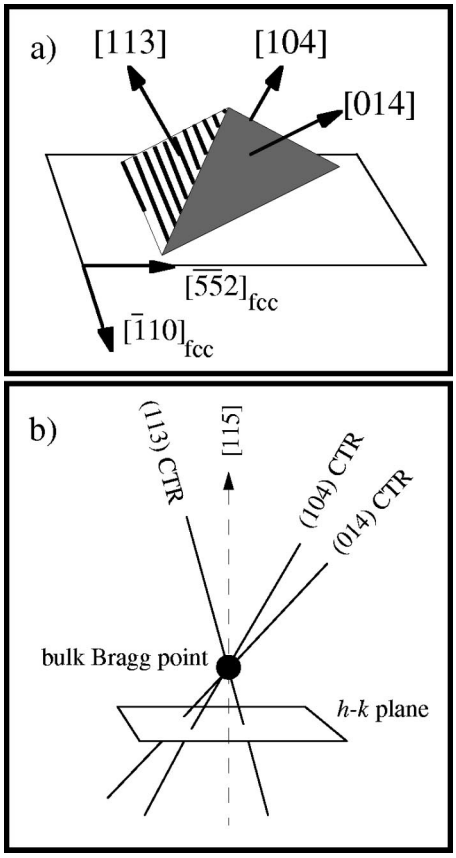

FIG. 2. (a) Direct-space view of the faceted O/Cu(115) surface (only one pyramid shown for clarity). (b) Reciprocal-space view around the $(111)_{fcc}=(603)_{115}$ bulk Bragg point. The CTR's are formed from the facets shown in (a); their orientations are determined by scans in the $h-k$ plane. Experimental STM images and reciprocal space maps by surface x-ray diffraction are shown in Refs. 31 and 21, respectively.

III. EXPERIMENTAL METHOD

This series of experiments was performed *in situ* at beamline X16A of the National Synchrotron Light Source, Brookhaven National Laboratory, on the five-circle UHV diffractometer.[85] The starting surface, clean Cu(115), was freshly prepared for each O-dosing experiment by sputtering with 1 keV Ar^+ ions followed by annealing to 550 °C. The sample temperature was then slowly lowered to a desired point (200 °C to 400 °C), and Cu(115) crystal truncation rods (CTR's) (Ref. 86) were measured to verify that the surface was clean, ordered, and free of other facets. O_2 was then admitted into the chamber through a leak valve at a constant partial pressure ($P_{O_2}=2\times10^{-9}$ Torr to 1.5×10^{-7} Torr). Figure 2(a) presents a schematic view of one facet pyramid on the resulting surface. CTR's from the faceted surface are shown in Fig. 2(b).

To observe the faceting process with diffraction, we continuously performed scans while dosing progressed. We scanned near the $(603)_{115}$ bulk Bragg peak, but close to the surface plane ($l=0.6$) to enhance surface sensitivity. [In this paper, we will work in (115) surface units, with h and k in the surface plane, and l normal to it. Thus, the $(603)_{115}$ Bragg point is $(111)_{fcc}$ in conventional reciprocal lattice units.] Since any well-defined facet on the surface will have a CTR associated with it,[87,88] its orientation can be determined from the direction in which its CTR points. Specifically, we determined orientations by locating the intersections of CTR's and the $l=0.6$ plane, using CTR's that originated at the $(603)_{115}$ Bragg point. The construction to do so is shown in Fig. 2(b). The primary scans were performed along $(h, 0, 0.6)$, to scan continuously from the (115) to (113) orientations. The scans effectively searched for all $(11n)$-oriented facets from $n\sim6$ to $n\sim2.5$. In several experiments, we also scanned radially and transversely through the (104) facet CTR. Our results, based on over 25 dosing experiments at various temperatures and O_2 partial pressures, are described in Sec. IV and interpreted in Sec. V.

IV. FACETING OBSERVED BY X-RAY DIFFRACTION

A. Early stage: (115) facet decomposition and (104) facet formation

Evolution of Cu(115) surface morphology during the early stage of O adsorption was qualitatively similar for the entire range of temperatures and O_2 partial pressures under consideration, and is described first. (Later effects, which vary strongly with substrate temperature, are described in Secs. IV B through IV D.) No immediate changes were observed in the (115) CTR as O dosing began, but slowly, the intensity of the CTR decreased without observable broadening or shifting of the peak; no facets other than (115) were observed in this time. This behavior is consistent with a random disordering of the steps on this surface,[89,82] similar to that observed for O on Cu($hk0$) vicinal surfaces.[90] Indeed, calculations by Jeong and Weeks[91] predicted that step fluctuations should increase (and step stiffness decrease, relative to an isolated step) for a vicinal surface undergoing spinodal decomposition.

Quite suddenly, however, the O-decorated Cu(115) surface destabilized and nanoscopic facets began to form. Two changes, occurring simultaneously, marked this transformation: the abrupt appearance of the O/Cu(104) and O/Cu(014) CTR's, and a gradual shift of the (115) CTR towards the (113) orientation. We index the intermediate facet as $(11n)$, with n representing the continuum of well defined but nonsingular orientations between (115) and (113), since the CTR remained moderately narrow but was not oriented along any high-symmetry direction. The tilting of the $(11n)$ CTR resulted from a shift in facet orientation away from (115) toward a more densely stepped surface. The gradual motion of the peak is shown for three dosing experiments in Fig. 3. The $(h, 0, 0.6)$ scans shown in Fig. 3 are a direct measure of facet orientation, since all of the rods pass through the $(603)_{115}$ bulk peak. The qualitative differences that arise with changing temperature are discussed below.

By repeating the O dosing experiments at many temperatures and pressures, we found a wide range in the time delay between initiation of O_2 dosing and the commencement of faceting, as shown in Fig. 4(a). Instead, we found that the *amount* of exposed O_2, i.e., dose rather than exposure time,

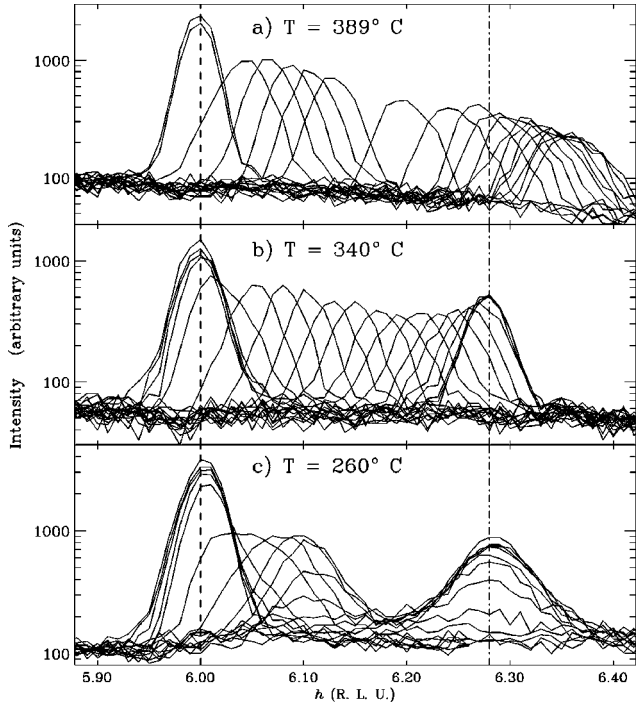

FIG. 3. Selected scans through $(11n)$ facet CTR's during faceting, for three representative temperatures. These scans are performed below the $(603)_{115}$ bulk peak, at $k=0$, $l=0.6$ in units of the 115 surface unit cell. The vertical dashed line indicates the (115) peak position ($h=6.0$), while the dot-dashed line marks the (113) peak position ($h=6.28$). Scanning proceeded from left to right, the same direction as peak motion, resulting in a slight broadening of the peaks. (a) $T=389$ °C; faceting did not cease at the (113) orientation. (b) $T=340$ °C; faceting proceeded smoothly from (115) to (113). (c) $T=260$ °C; faceting occurred discontinuously from (115) to (113). In contrast to this behavior, the (104) facet's CTR exhibits no changes in position, simply growing (with increasing dose) at the exact (104) position for all temperatures investigated [see Figs. 8(c)–8(d)].

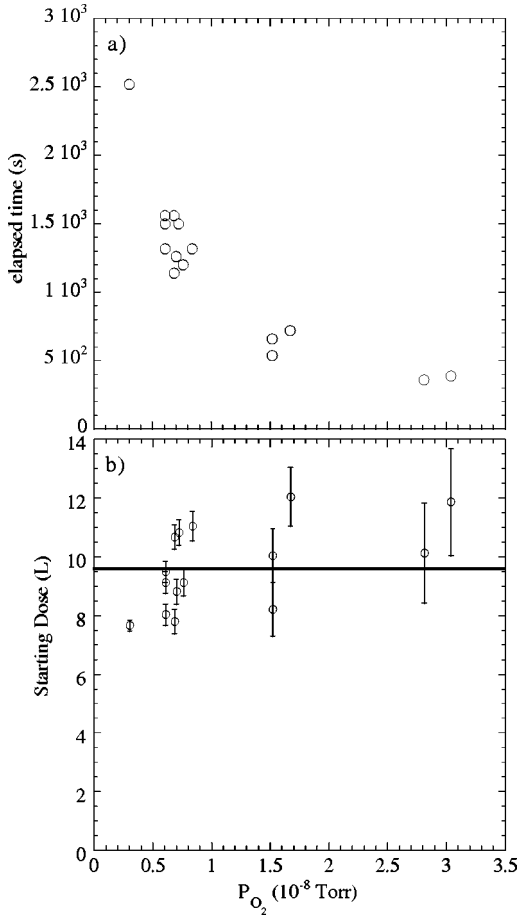

FIG. 4. Plots of (a) elapsed time and (b) O_2 dose at which faceting began, which turns out to be a dose of 9.6 L. The beginning of faceting is defined as the point at which the (115) facet peak began to move towards (113).

was the critical factor to initiate faceting. For the entire range of pressures and temperatures studied in these experiments, faceting began after an exposure of 9.6 ± 1.4 L of oxygen, as shown in Fig. 4(b). The ''starting dose'' is defined as the dose at which the (115) CTR peak developed a clear shoulder on the high-h side. An alternative definition of ''starting dose'' could be the exact dose at which the (104) facet CTR first appeared. That definition is less practical to employ; the change in position (or line shape) of an existing peak is easier to observe than the appearance of a new peak out of the diffuse background. However, we find the two definitions to be equivalent to within measurement uncertainty (±2 L) when we project the early-time (104) CTR intensities [shown in Fig. 8(c)–8(d)] back to zero intensity.

In our measurements, the starting dose could be most accurately determined when changes in surface morphology were the slowest, i.e., at lower O_2 partial pressures. This accounts for the larger error bars associated with the higher pressures of Fig. 4(b); other experiments at even higher partial pressures cannot be included in Fig. 4 because faceting occurred too quickly to accurately determine the starting dose. Since the temporal evolution of the faceting surface was observed to depend on cumulative O_2 exposure (rather than exposure time), in the following sections we will plot any changes to the facets against O_2 dose instead of exposure time. This will normalize experiments performed at different O_2 partial pressures. Faceting was typically completed after a total dose of 30 to 40 L independent of temperature or pressure (except for the highest temperatures, as described below), but the time scales could range from minutes to hours depending on P_{O_2}.

The observation that faceting began after a 9.6-L dose is consistent with STM micrographs taken by Taglauer *et al.*[92] at 210 °C as a function of dose: After an O_2 exposure of 10 L, the Cu(115) surface was somewhat disordered and a moderate fraction of the surface area was faceted. The surface was completely transformed to (104), (014), and (113) facets after a 30-L exposure, although facet sizes continued evolving after higher doses.[92] A follow-up STM study[33] showed that facet density increased with increasing P_{O_2}, further evidence that faceting began by O-limited nucleation (i.e., higher P_{O_2} leads to more nucleation sites and thus more facets).

The observed behavior of the (104) and (014) facets differed significantly from that of the $(11n)$ facets. The CTR's associated with the (104) facets were always found at the exact (104) orientation, never shifting position. The (104) CTR peaks did gain intensity, reflecting the spread of these facets across the surface until the $(11n)$ facet ceased evolving; this behavior of the (104) facets was consistently found for all temperatures studied. The (113) facets, as mentioned above, did not form abruptly; furthermore, their evolution was strongly temperature dependent. In Secs. IV B through IV D, we describe the behavior found for each temperature regime.

B. Medium-temperature (113) facet formation

We first discuss (113) facet growth in the medium temperature regime ($310\,^{\circ}\mathrm{C} \lesssim T \lesssim 370\,^{\circ}\mathrm{C}$), since the phenomenon was most straightforward here. For all experiments performed in this temperature range, the sequence of peak profiles is qualitatively similar when scaled to dose (but not, as discussed above, time). Just as the {104} facet peak appeared, the (115) peak shifted in the $+h$ direction away from its original position of $h=6$, as seen in Fig. 3(b). In some dosing experiments, the $(11n)$ peak begins as a clear shoulder on the side of the (115) peak; this behavior is seen easiest at low temperatures but occurs in all temperature regimes. No lateral peak shift was ever observed in k. The change in peak position in h corresponded to a change in the orientation of the $(11n)$ facet, with n changing smoothly from five to three in this temperature regime. To better visualize the evolution of the $(11n)$ facets, the facet positions from Fig. 3 are plotted against O_2 exposure in Fig. 5. Peak position in h for a given l (the left axes of Fig. 5) is a direct measure of facet orientation; thus, the facet's angular deviation from (115) can be shown on the right axes. The symbol size in this figure reflects peak height from Fig. 3.

In this middle temperature regime, the $(11n)$ facet peak was moderately broader than the initial (115) peak but remained sharp, reflecting a well defined yet continuously changing orientation as the (104) and (014) facets grew. The widths of the $(11n)$ peaks are given by a combination of the facet size, the small range of facet orientations, and instrumental resolution (including the effect of scans being performed along the direction of peak motion, see Fig. 3). The shifting of the $(11n)$ orientation was due to a gradual bunching of steps on the $(11n)$ facets, with the average step separation changing from 6.64 Å [for Cu(115)] to 4.24 Å [for Cu(113)]. This mode of step formation may help explain the structural disorder found on the O/Cu(113)(3×1) facets (see Refs. 21 and 31).

Once faceting concluded and the (113) peak had formed, we found that the size of the facets (inversely proportional to the CTR widths) tended to be greater at higher temperatures (as long as $T<370\,^{\circ}\mathrm{C}$). This is seen in the significantly broader (113) peak at $T=260\,^{\circ}\mathrm{C}$ [Fig. 3(c)] compared to the (113) peak at $T=340\,^{\circ}\mathrm{C}$ [Fig. 3(b)], even though the initial (115) peaks at the two temperatures were about equal in width. Similar results on the final facet size have been quantified with STM.[33]

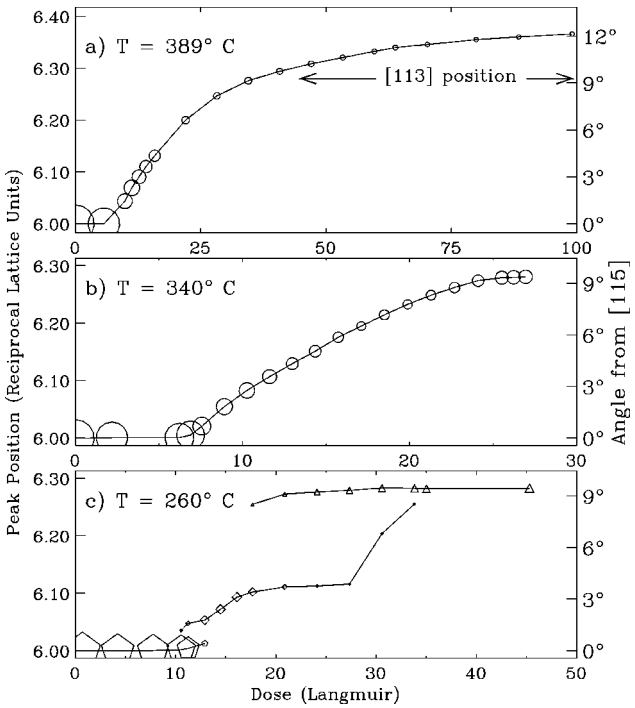

FIG. 5. Positions of $(11n)$ facets shown in Fig. 3 during dosing. The radius of the symbol is proportional to the height of the facet peak. The left axis gives peak position in 115 reciprocal lattice units, and the right gives the angle of the facet from (115) [which is 9.45° for (113)]. In (a) and (b) ($T=389\,^{\circ}\mathrm{C}$ and $340\,^{\circ}\mathrm{C}$, respectively), circles represent the position of the $(11n)$ facet peak as it changes smoothly to (113) (and beyond, for $T=389\,^{\circ}\mathrm{C}$). In (c) ($T=260\,^{\circ}\mathrm{C}$), pentagons refer to the (115) peak position, diamonds to the $(11n)$ peak, and triangles to the (113) peak.

C. High-temperature $(11n)$ facet formation

The beginning of the faceting process at high temperatures ($T \gtrsim 370\,^{\circ}\mathrm{C}$) is qualitatively similar to the medium-temperature regime. The change in orientation through the $(11n)$ facets was continuous [the scans in Fig. 3(a) are not equally spaced in time]; the difference is that the peak continued well past the (113) position. Even after a dose of 100 L, the orientation of the facet continued to progress away from (115), although the rate of peak motion had slowed considerably. In terms of the Wulff plot, this behavior demonstrates the complete removal of a cusp at (113), as discussed in detail below.

D. Low-temperature (113) facet formation

The formation of (113) facets at low temperatures ($T \lesssim 310\,^{\circ}\mathrm{C}$) differed significantly from the previous cases. After a dose of ~ 10 L, the {104} facets formed suddenly, as above, but the $(11n)$ facet did not smoothly shift in orientation, as seen in Fig. 3(c). The $(11n)$ peak clearly began as a shoulder to the (115) peak, but did not proceed continuously to $n=3$. It moved less than halfway to the (113) position and then dropped in intensity while the (113) peak abruptly appeared. In sharp contrast to the results at higher temperatures, no well-defined peak was observed for the range of orientations around $h=6.2$, or angles $\gtrsim 4°$ from (115). In-

stead, *two* peaks were present for part of the dosing time; thus, the faceting surface at lower temperatures consisted of coexisting domains of (113) and $(11n)$ orientations, with the (113) facets growing at the expense of the $(11n)$ facets. This behavior does not necessarily indicate an increase in the surface free energy of some $(11n)$ orientations; rather, as detailed in Sec. V A, it is due to a decrease in the surface free energy at (113).

The (113) CTR did not change orientation once the $(11n)$ facet had disappeared, but a moderate increase in intensity and narrowing of width was typically observed. This effect, more pronounced at lower temperatures, reflected the slow ordering that took place on this moderately disordered[21] surface. The ordering was slowest and least complete at lowest temperatures, where surface diffusion was slowest. No corresponding effect was observed for the (104) CTR's, which did not seem to change in intensity or width once the $(11n)$ facet peak disappeared.

E. Reversal of faceting

Once the (113) facets had formed and surface evolution had ceased, we observed that the faceted surface was stable even when oxygen gas was removed from the chamber. Facets decomposed only upon annealing at 500 °C, at which point O desorption from the fully faceted surface became significant. We also performed a few experiments wherein the O supply was cut off after faceting had begun, but well before (113) facets had formed. Specifically, during a dose at $T=263$ °C and $P_{O_2}=8\times10^{-9}$ Torr, the O_2 supply was cut off when the $(11n)$ peak had reached $h=6.08$; faceting did not continue or even cease, but immediately *reversed*, reverting to the (115) orientation without the development of any other facets. This (115) surface was moderately well ordered, as judged by CTR intensities and widths, but was not as good as a freshly prepared (115) surface. In another case, O dosing in the high-temperature regime ($T=389$ °C, $P_{O_2}=1.5\times10^{-8}$ Torr) was cut off with the $(11n)$ peak at $h=6.36$ [namely, just after the last scan in Fig. 3(a)]; reversal of orientation was again immediate, and we note that this surface showed no tendency to stabilize at the (113) facet, but continued back towards (115). The immediate reversal of facet formation is directly attributable to oxygen desorption. But as a surface with multiple, crystallographically inequivalent facets is not well suited for a quantitative study of desorption kinetics, this series of experiments was not pursued further.

V. STABILITY AND EVOLUTION OF FACETS

A. Equilibrium surface-free energies of facets

The real-time experiments described in Sec. IV dramatically demonstrate the sensitivity of the O/Cu(115) faceting process to substrate temperature and O_2 dose, but its relative insensitivity to O_2 partial pressure. From these results, we are able to describe the relative stabilities of a number of orientations near the O/Cu(115) pole and determine the long-time evolution of the faceting surface. Such results are possible because the surface structure remains, locally, in equilibrium as the surface undergoes spinodal decomposition from (115) to (104), (014), and (113) facets. While the oxygen in vapor form is not in equilibrium with the oxygen adsorbed on the surface, we argue that the surface morphology is always in equilibrium for a given oxygen coverage.

Several observations show that adsorbate-induced faceting in this system is not merely a kinetic effect. First of all, Sec. IV A demonstrates that, for all temperatures and pressures investigated, faceting begins after a nonzero O_2 dose, i.e., after a certain amount of oxygen had adsorbed onto Cu(115). A kinetically activated process would likely be observed to begin immediately, or would exhibit a temperature-dependent time delay, rather than a temperature-independent dose delay. Second, continued oxygen adsorption was essential for faceting to continue. As described in Sec. IV E, the removal of O_2 from the vacuum chamber immediately caused the facets to decompose; a kinetic effect might cause facet evolution to stall without O_2 but would not reverse the process. We also note that the role of oxygen is not primarily that of a surfactant, i.e., to increase the mobility of Cu adatoms; previous experiments[93,94] have demonstrated the high mobility of Cu on low-symmetry Cu surfaces without oxygen present, and at substantially lower temperatures. The oxygen, then, changes the surface free energies of various facet orientations, forcing the surface to undergo spinodal decomposition as O coverage increases.

The primary effect of O on the Cu(115) surface, then, is to lower the surface free energy of the (104) facet, which results in an increase to the anisotropy of the Wulff plot. As discussed in Sec. II, faceting can become energetically favorable for a sufficiently anisotropic Wulff plot, despite the accompanying increase in surface area. In the present series of experiments, O/Cu(104) facets were observed for all faceting temperatures and O_2 partial pressures; these facets formed abruptly and were never misoriented. Therefore, we conclude that formation of O/Cu(104) facets drives the faceting of the Cu(115) surface, consistent with previous studies on Cu(115) and other Cu(001) vicinal surfaces. The stability of this facet has been attributed to its structural similarity to a regularly stepped version of the O/Cu(001)$(2\sqrt{2}\times\sqrt{2})$ surface;[95] this concept may be tested rigorously now that the O/Cu(104) structure is known.[21]

Once the O/Cu(104) facets begin to form and grow, the $(11n)$ facets must evolve in order to maintain a macroscopic (115) orientation. Therefore, O/Cu(115) facets cannot remain on the surface, but it does not necessarily follow that these facets become intrinsically unstable. Boulliard *et al.*[28] observed a weak LEED pattern from (115) facets after O-induced faceting of Cu(117) at high coverages and low temperatures (200 °C). O/Cu(115) could thus be locally stable but, like orientation *B* in Fig. 1, be overwhelmed by nearby orientations with much lower surface free energies.

The evolution of the $(11n)$ facet orientation is thus driven by the growth of the (104) facets, essentially via step bunching. That is, as the (104) facets grow, the $(11n)$ facets must tilt farther and farther from (115) in order to maintain an overall (115) orientation for the macroscopic surface. This tilting involves a significant amount of mass transport of Cu atoms at and near the surface, which in this UHV experiment

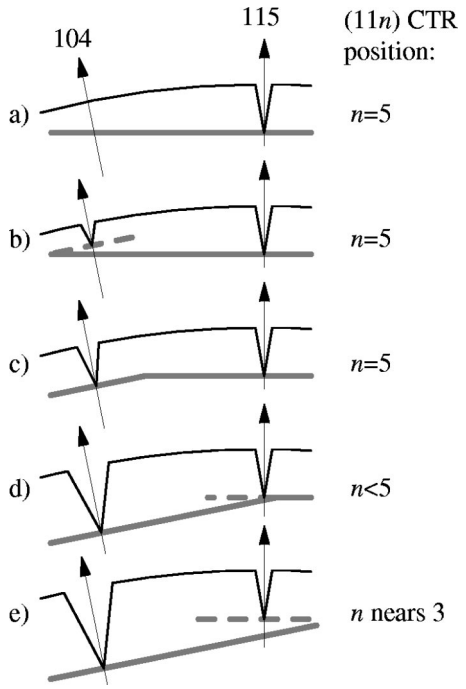

FIG. 6. Proposed dose-dependent Wulff plots for orientations between (115) and (104) [or equivalently, (014)], with dose increasing from (a) to (e). The thin black line is the surface-free energy, while the thicker grey line is the equilibrium crystal shape. Broken grey line represents facets that do not appear on the equilibrium crystal shape.

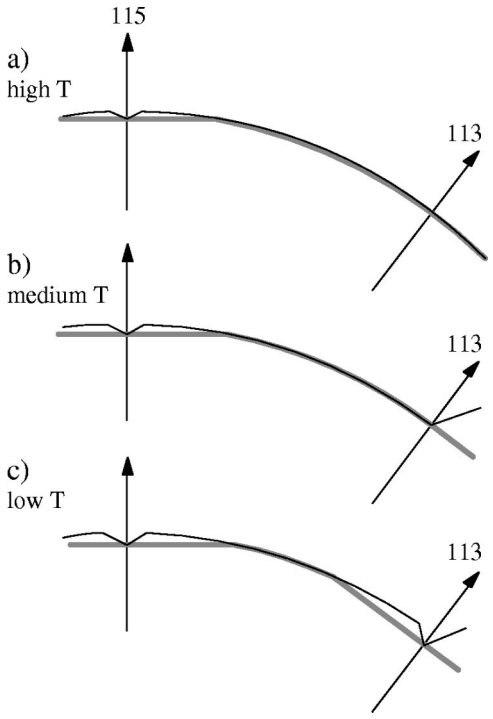

FIG. 7. Proposed Wulff plots for O/Cu(11*n*) in three temperature regimes. (a) $T \gtrsim 370\,^{\circ}\mathrm{C}$; (b) $310\,^{\circ}\mathrm{C} \lesssim T \lesssim 370\,^{\circ}\mathrm{C}$; (c) $T \lesssim 310\,^{\circ}\mathrm{C}$. Thin black line: Surface-free energy [assumed constant, except for temperature-dependent cusps at (113) and (115)]. Thicker, grey line: Equilibrium crystal shape. The angular separation of the (115) and (113) directions and the depth of the (115) cusp are greatly exaggerated for visibility.

occurs by surface diffusion (rather than bulk diffusion or evaporation condensation). The details of this evolution, however, are sensitive to the surface free energies of the O-covered (11*n*) facets. Figure 5 displays the contrasting behaviors of (11*n*) facet evolution in the three temperature regimes; the faceting is driven by the changing surface free energy of (104), with the temperature variations determined by the changing surface free energy at (113). To present concisely the variations in surface free energy with orientation and temperature, we propose two sets of Wulff plots around the (115) pole for the O on Cu system.

First we present schematic *dose*-dependent Wulff plots for orientations between (104) and (115) in Fig. 6. Increasing O_2 exposure progresses from Figs. 6(a) to 6(e). Figure 6(a) shows a Wulff plot for clean Cu, with a cusp at (115), denoting that facet's stability, but no cusp at (104), although a tiny one could in principle exist there. Clean Cu(104) is a relatively unstable facet that disorders easily. Intermediate orientations have much higher Miller indices and no expected tendency for stability. Figures 6(b) and 6(c) are Wulff plots for O_2 coverages between 0 and 9.6 L; although a cusp may be present at (104), at first it is not deep enough to induce a stable facet [Fig. 6(b)]. Next, even when a (104) facet is stable [Fig. 6(c)], the (104) cusp is not deep enough to overwhelm the cusp at (115). At a sufficiently high coverage, the (104) facet indeed overwhelms the (115) facet [Fig. 6(d)], forcing the latter to change its orientation slowly towards (113) as O_2 coverage [and the depth of the (104) cusp] further increases [Fig. 6(e)]. Thus, the average orientation of the (11*n*) facet tracks the depth of the (104) cusp; the time dependence of the facet evolution is described below in Sec. V B. With a simple geometric construction based on Fig. 6, we can compare the surface free energies of the (104) and (115) orientations (γ_{104} and γ_{115}, respectively) at the point where the (115) facet becomes unstable. With θ_{miss} representing the angular width of the missing orientations,

$$\gamma_{104} = \cos\theta_{\mathrm{miss}}\,\gamma_{115} = 0.980\,\gamma_{115}, \tag{3}$$

since in this case $\theta_{\mathrm{miss}} = 11.4°$, the angle between (104) and (115). We emphasize that Eq. (3) is valid only at the very point at which faceting begins, a dose of 9.6 L.

The dose-dependent Wulff plots presented in Fig. 6, for orientations between (104) and (115), are independent of temperature, since the early stage of faceting was uniform for the range of temperatures covered in this study. However, Figs. 3 and 5 demonstrate a significant *temperature* dependence to the Wulff plots of orientations between (115) and (113), which we display in Fig. 7. In proposing these (11*n*) Wulff plots, we assume the surface free energy of these orientations does not vary with coverage for doses over 10 L, i.e., once the (11*n*) orientations have appeared. For all temperature regimes, the surface free energy γ_{11n} can be considered constant for $5 > n > 3$. The nonzero cusp at (115) removes (11*n*) orientations, with *n* very close to 5, from the equilibrium crystal shape; this small range of missing orientations is more clearly present in the low-temperature experi-

ments [Fig. 3(c)] than at higher temperatures [Figs. 3(a) and 3(b)]. While we expect a small, residual (115) cusp at all temperatures, we note that its depth as pictured in Fig. 7 is severely exaggerated.

The main difference between the Wulff plots of the high- and medium-temperature regimes is for $n<3$. For high temperatures [Fig. 7(a)] there is no apparent change in the surface free energy from $n>3$, allowing the orientation to smoothly move further and further away from (115) as the (104) cusp grows deeper. But for medium temperatures [Fig. 7(b)], a tiny cusp seems to exist at (113), and the surface free energy of $n<3$ is greater than that for $n>3$; this has the effect of stabilizing the (113) surface and halting facet growth even if the (104) cusp continues to deepen with time. The extent to which the surface free energy increases for $n<3$ is not measurable here since we do not observe these orientations in this temperature range. A cusp must exist at (113) for medium temperatures, since removal of oxygen from the chamber did not lead to the (113) facets decomposing. However, the depth of the (113) cusp must be very small since we were not able to observe a range of missing orientations around (113), as we were able to do at low temperatures.

In the low-temperature regime [Fig. 7(c)], a relatively deep cusp is definitely present at (113), which causes a large range of orientations to disappear from the equilibrium crystal shape. The origin of this cusp is likely to be the (3×1) reconstruction observed for O/Cu(113).[21] The range of missing orientations [with angles up to 6° from (113)], was constant from $200\,^{\circ}\mathrm{C}<T<310\,^{\circ}\mathrm{C}$ but disappeared above 310 °C. The abrupt disappearance of the missing region is indicative of a first-order phase transition in the surface free energy at 310 °C, i.e., the near disappearance of the cusp in raising the temperature from Figs. 7(c) to 7(b). We hypothesize that this phase transition may coincide with the removal of the (3×1) orientation at 310 °C. As above with Eq. (3), a simple geometric calculation allows us to determine the surface free energy of the (113) cusp at low temperature γ_{113} compared with the surface free energy of a nonsingular point along $(11n)$ γ_{11n} (constant for $5>n>3$):

$$\gamma_{113}=\cos\theta_{\mathrm{miss}}\,\gamma_{11n}\sim0.995\,\gamma_{11n}, \tag{4}$$

since θ_{miss} is about 6° for $T<310\,^{\circ}\mathrm{C}$. Again, we note the scale of Fig. 7 is exaggerated for clarity, and that the cusp at (113) is much deeper than the cusp at (115). The range of missing orientations at (115) is at most 1° [see Fig. 5(c)]. Thus, $\gamma_{11n}-\gamma_{115}\lesssim0.001\,\gamma_{11n}$ at 260 °C, and even smaller at higher temperatures.

B. Dynamic scaling of facet growth

Beyond the preceding description of the orientational dependence of surface free energies, the measurement of facet orientation vs O_2 exposure can explore the dynamic scaling of the facets as they undergo spinodal decomposition. Two order parameters can be used to describe the state of the faceting surface and present complementary information on the complex process of facet growth: I_{104}, the intensity of the (104) CTR at a given point, can be related to the surface area covered by (104) facets, and the $(11n)$ facet orientation can be related to the relative sizes of the (104) and $(11n)$ facets, as described below. As we use these parameters, we will explicitly enumerate the necessary assumptions that are used in deriving scaling relations.

We first analyze dynamic scaling based on the orientation of the $(11n)$ facets in the middle- and high-temperature regimes. The relative area of the (104) facets based on the $(11n)$ facet orientation can be evaluated by employing the laws of conservation of projected surface area and of macroscopic orientation.[96] We take S_{104}/S_{115} to be the surface area of the (104) facets [projected onto the (115) surface] relative to the starting (115) area. As detailed elsewhere,[87] S_{104}/S_{115} can be expressed in terms of the $(11n)$ facet orientation, or equivalently in terms of h, the position (in reciprocal lattice units) of the $(11n)$ peak at a given l (as in Fig. 3, where $l=0.6$). However, two conditions must be met in order for S_{104}/S_{115} to be a useful scaling parameter: first, the entire surface must be faceting at about the same rate; second, the area covered by the faceting pyramids must remain constant during a dosing experiment. The first condition requires that only well-defined (104), (014), and $(11n)$ facets be found on the surface while faceting occurs, with no other facet present. This has been experimentally verified for the middle- and high-temperature faceting regimes, as described in Secs. IV B and IV C. It is clearly not met in the low-temperature regime (Sec. IV D), since the distribution of $(11n)$ orientations becomes bimodal about halfway through the faceting process when (113) facets appear. The second condition is needed to ensure that S_{104}/S_{115} is a measure of the growing *size* of the (104) facets, instead of a changing *number* of (104) facets. Although some small amount of ripening probably occurs, we observed the (104) facet peak to always cease evolving when the $(11n)$ facet reached (113). This proves that the (104) facets grow in size mainly at the expense of the $(11n)$ orientation, not at the expense of other (104) or (014) facets. Any scaling in the middle temperature regime will, of course, be abruptly truncated when the $(11n)$ facet reaches (113) and ceases evolving.

The results of scaling based on $(11n)$ orientation are shown for two experiments in Figs. 8(a)–8(b). The normalized area S_{104}/S_{115} is plotted against dose for typical dosing experiments at medium and high temperatures. These experiments were performed at different but relatively low-oxygen partial pressures, since slower changes in morphology could be traced with higher resolution. In addition, we have plotted the best fits of logarithmic $[\log(t-t_0)]$ and power-law $[(t-t_0)^{\phi}]$ scaling over the later stages of faceting. The ''starting dose'' t_0 (see Sec. IV A and Fig. 4) was included as a fitting parameter, since it could not be measured precisely. We find that both scaling forms produce very good fits to the available data, with the fits being of essentially equal quality. Furthermore, for the power-law fits, there is a rather large range in the fit to the exponent ϕ, from 0.11 to 0.25. The limited information that can be derived from these fits is directly due to the relatively short time spans over which faceting occurs: faceting is abruptly truncated when the (113) facet is reached, necessarily limiting the fittable range and the ability to discriminate between alternative models.

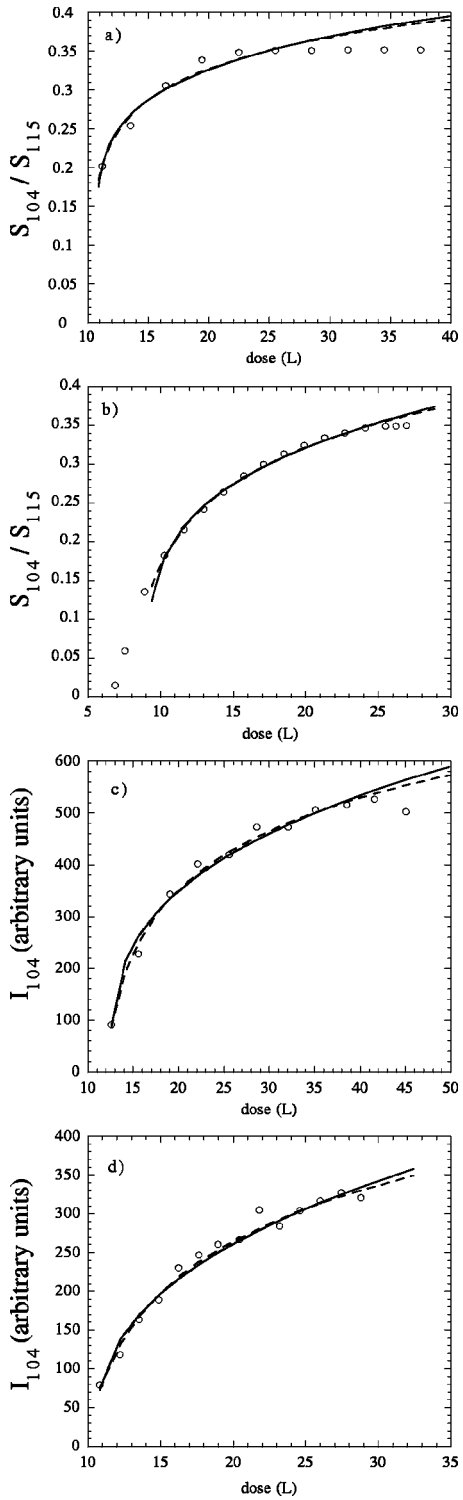

FIG. 8. Dynamic scaling of O/Cu(104) facet size during O_2 exposure. In all plots, circles are measurements; solid and dashed lines are best fits to logarithmic and power-law scaling, respectively. (a)–(b) Scaling by projected area of (104) facets. (a) Dosing with experimental conditions of $T=336\,^{\circ}\mathrm{C}$ and $P_{O_2}=2\times10^{-8}$ Torr. The resulting power-law fit yields $\phi=0.17\pm0.04$. (b) $T=340\,^{\circ}\mathrm{C}$, $P_{O_2}=3\times10^{-9}$ Torr; $\phi=0.26\pm0.02$. (c)–(d) Scaling by intensity of (104) CTR (c) $T=260\,^{\circ}\mathrm{C}$, $P_{O_2}=8\times10^{-9}$ Torr; $\phi'=0.33\pm0.03$. (d) $T=340\,^{\circ}\mathrm{C}$, $P_{O_2}=3\times10^{-9}$ Torr; $\phi'=0.38\pm0.03$. Further data are presented in Ref. 87.

Although the scaling in Figs. 8(a)–8(b) was performed with respect to calculated area of the (104) facets, these results essentially represent the growth of the facets in linear size. That is, $S_{104}\propto L_xL_y$ where L_x and L_y are the length and width of the (104) facets (with x perpendicular to and y parallel to the $\langle010\rangle$-type steps on this surface), but the evolution of S_{104}/S_{115} mainly reflects the evolution of L_x. This is because (104) facet growth is anisotropic: a given facet grows very quickly along its $\langle010\rangle$-type rows (parallel to the O-Cu-O rows), but much slower across the rows. While the widths of the (104) CTR's were quite broad in x, the widths in y were much narrower (indicative of longer-ranged order) and were not observed to change while faceting occurred.[21] Therefore, the evolution of L_y finished rapidly, and the facets grew in area mainly by the increase in L_x. Such growth rate anisotropies have been previously observed experimentally[61] and theoretically.[84]

As a separate measure of the size of the (104) facets, we have investigated the evolution of I_{104}, the scattered intensity at a point on the (104) CTR. Specifically, in Figs. 8(c)–8(d) we plot the peak intensity (above background) at the point $(5,1,1.06)_{104}$ against dose. For several experiments in the low- and middle-temperature regimes, the intensity is fit about equally well by either logarithmic or power-law scaling (with exponent ϕ'). Again, this scaling only occurs up to the point at which the (113) orientation is reached and faceting ceases, whereupon I_{104} saturates. We note that the evolution of I_{104} with dose is smooth and gives no sign of the discontinuities of the $(11n)$ evolution at low temperatures [in, e.g., Fig. 5(c)]. Although the mix of $(11n)$ and (113) orientations prohibited reliable calculation of S_{104}/S_{115} in the low-temperature regime, we can use I_{104} to study dynamical scaling for those experiments.

The CTR intensity I_{104} can be related to the number of (104) facets on the surface N_f and to the average length and width of the facets (L_x and L_y, respectively) by

$$I_{104}\propto|F_{104}|^2N_f(L_xL_y)^r, \tag{5}$$

and will be a useful scaling parameter if it varies only with facet length. As we argued above, N_f and L_y changed little in the later stages of faceting [due to the uniform faceting rate across the surface and to the anisotropic growth of the (104) facets, respectively]. Furthermore, we assume that F_{104}, the structure factor of the (104) CTR at the point of measurement, is constant during faceting. That is, the surface structure of the (104) facets does not change, due to their greater stability (which drives the spinodal decomposition of the surface in the first place). Thus, I_{104} varies as $(L_x)^r$, with $r=1$ in the resolution limit, and $r=2$ in the particle-size broadening limit. Unfortunately, the experimental situation is likely somewhere in between: $1<r<2$. As such, the power-law exponents fitted in Figs. 8(c)–8(d) are equal to $\phi'=r\phi$. Taking $r=2$ gives the lower bound of ϕ; the average value for ϕ, with this assumption, is then 0.16, which is consistent with scaling by S_{104}/S_{115}. On the other hand, $r=1$ is consistent with logarithmic scaling of L_x, but $r=2$ is not (since I_{104} could not be fit as a square logarithm).

If we combine the results of the power-law scaling of S_{104}/S_{115} and I_{104}, then the best estimate of the exponent (given the limited range of dynamic scaling for each dosing experiment) is 0.17 ± 0.03. This low value is consistent with other faceting experiments[59,42] performed on other, very different low-symmetry surfaces. We emphasize, however, the difficulty in differentiating power-law scaling with small exponents from logarithmic scaling. Logarithmic scaling would be consistent with one-dimensional diffusion[81] and with diffusion lengths that grow with the facet size,[83] either of which could be expected for faceting on this vicinal surface. However, as noted above, the faceting process as a whole scales more with O_2 dose than with time alone. The limiting factor in the dynamical scaling (whether as a power law or as a logarithm) is, then, the depth of the (104) cusp as a function of time. The depth of this cusp is determined by the rate of incorporation of O_2 onto the surface, which is directly proportional to the availability of oxygen, i.e., the partial pressure of O_2. The mass transport required for the surface to maintain its equilibrium shape as a function of dose occurs on relatively shorter time scales. This conclusion cannot be drawn from a single measurement, but is seen in the pressure dependence of the experiments discussed in Sec. IV A. The one experiment that provides a direct comparison of scaling by S_{104}/S_{115} and I_{104} ($T = 340\ ^\circ\mathrm{C}$) gives moderately different values for ϕ:0.26 [Fig. 8(b)] vs 0.19 [Fig. 8(d)], respectively. This difference is greater than the fitted uncertainty, and could be an indirect argument for logarithmic fitting. But it is as likely due to a breakdown in the assumption that $r = 2$, that facet diffraction is at the particle-size limit, is in error; a smaller value of r would raise the resulting value of ϕ from 0.19.

VI. CONCLUSION

We have used surface x-ray diffraction to observe the process of oxygen-induced faceting of Cu(115) in real time. We confirmed that faceting is driven by the formation of the O/Cu(104) and (crystallographically equivalent) O/Cu(014) facets, and more specifically found the faceting rate is determined by the depth of the Wulff plot's cusp at (104) relative to (115). The gradual deepening of the (104) cusp with O_2 dose explains all features of the time dependence of the faceting process, including the delay of about 10 L before faceting begins. On the other hand, the temperature dependence of the O/Cu(113) orientation's surface free energy determines the complicated evolution of the facets along $(11n)$. The low symmetry of this faceted surface (i.e., three-sided pyramids with only two crystallographically equivalent sides) certainly complicates the faceting process, but the temperature-dependent Wulff plot along $(11n)$ is clearly an effect subordinate to the dose dependence at (104). Relative values for the surface free energy were presented for orientations that are separated by a range of forbidden orientations.

Two independent parameters are sensitive to (104) facet size, and thus, to the dose dependence of the surface free energy of O/Cu(104). The dynamic scaling of these parameters was not unambiguously resolved but was either logarithmic or power law with a small exponent, in either case reflective of slow facet evolution. We have proposed that the time evolution for this case of adsorbate-induced faceting is limited, and thus governed, by the rate of decrease of a particular orientation's surface free energy. The depth of the cusp at (104), i.e., the stability of O/Cu(104) facets, increases with O_2 exposure; thus, the timescale of this faceting mechanism is set by adsorbate incorporation rather than being limited by surface-diffusion kinetics (the more commonly assumed case for facet growth). It would be interesting to see whether other faceting experiments, e.g., O-induced faceting on other Cu high-index surfaces, have time scales set by changes in the equilibrium crystal shape, and thus, yield similar time (or dose) dependencies.

ACKNOWLEDGMENTS

We thank H. Meyerheim for use of the Cu(115) crystal. This research was supported by NSF Grant No. DMR 98-76610. The NSLS is supported by the U.S. Department of Energy under Grant No. DE-AC02-98CH10886.

*Present address: Department of Materials Science and Engineering, Northwestern University, 2225 North Campus Drive, Evanston, IL 60208.

[1] M. Flytzani-Stephanopoulos and L.D. Schmidt, Prog. Surf. Sci. **9**, 83 (1979).
[2] J. Falta, R. Imbihl, and M. Henzler, Phys. Rev. Lett. **64**, 1409 (1990).
[3] G.A. Somorjai, J. Mol. Catal. A: **107**, 39 (1996).
[4] V.P. Zhdanov and B. Kasemo, Phys. Rev. Lett. **81**, 2482 (1998).
[5] S. Johansson, K. Wong, V.P. Zhdanov, and B. Kasemo, J. Vac. Sci. Technol. A **17**, 297 (1999).
[6] J. Onsgaard, S.V. Hoffmann, P.J. Godowski, P. Moller, J.B. Wagner, A. Groso, A. Baraldi, G. Comelli, and G. Paolucci, Chem. Phys. Lett. **322**, 247 (2000).
[7] P. Marcus, Electrochim. Acta **43**, 109 (1998).
[8] D.R. Giese, F.J. Lamelas, H.A. Owen, R. Plass, and M. Gajdardziska-Josifovska, Surf. Sci. **457**, 326 (2000).
[9] H. Schubert, U. Tegtmeyer, D. Herein, X. Bao, M. Muhler, and R. Schlögel, Catal. Lett. **33**, 305 (1995).
[10] A. Berkó, G. Ménesi, and F. Solymosi, J. Phys. Chem. **100**, 17 732 (1996).
[11] H. Graoui, S. Giorgio, and C.R. Henry, Surf. Sci. **417**, 350 (1998).
[12] M. Wortis, in *Chemistry and Physics of Solid Surfaces VII*, edited by R. Vanselow and R. Howe (Springer-Verlag, Berlin, 1988), p. 367.
[13] N.A. Gjostein, Acta Metall. **11**, 957 (1963).
[14] N.A. Gjostein, Acta Metall. **11**, 969 (1963).
[15] A. Shi, Phys. Rev. B **36**, 9068 (1987).
[16] J.K. Nørskov, Rep. Prog. Phys. **53**, 1253 (1990).
[17] G.R. Darling and S. Holloway, Rep. Prog. Phys. **58**, 1595 (1995).
[18] J.L. Whitten and H. Yang, Surf. Sci. Rep. **24**, 55 (1996).

[19] M. Papoular, Europhys. Lett. **33**, 211 (1996).
[20] E.D. Williams and N.C. Bartelt, Science **251**, 393 (1991).
[21] D.A. Walko and I.K. Robinson, Phys. Rev. B **59**, 15446 (1999).
[22] W. Berndt, Z. Naturforsch. A **22A**, 1655 (1967).
[23] L. Trepte, C. Menzel-Kopp, and E. Menzel, Surf. Sci. **8**, 223 (1967).
[24] J. Perdereau and G.E. Rhead, Surf. Sci. **24**, 555 (1971).
[25] E. Legrand-Bonnyns and A. Ponslet, Surf. Sci. **53**, 675 (1975).
[26] K.A. Thompson and C.S. Fadley, Surf. Sci. **146**, 281 (1984).
[27] J.C. Boulliard, C. Cohen, J.L. Domange, A.V. Drigo, A. L'Hoir, J. Moulin, and M. Sotto, Phys. Rev. B **30**, 2470 (1984).
[28] J.C. Boulliard, J.L. Domange, and M. Sotto, Surf. Sci. **165**, 434 (1986).
[29] M. Sotto, Surf. Sci. **260**, 235 (1992).
[30] G.W. Lloyd and D.P. Woodruff, Surf. Sci. **285**, L503 (1993).
[31] S. Reiter and E. Taglauer, Surf. Sci. **367**, 33 (1996).
[32] P.J. Knight, S.M. Driver, and D.P. Woodruff, J. Phys.: Condens. Matter **9**, 21 (1997).
[33] N. Reinecke and E. Taglauer, Surf. Sci. **454–456**, 94 (2000).
[34] J.C. Tracy and J.M. Blakely, Surf. Sci. **13**, 313 (1968).
[35] J.S. Ozcomert, W.W. Pai, N.C. Bartelt, and J.E. Reutt-Robey, Phys. Rev. Lett. **72**, 258 (1994).
[36] R.J. Phaneuf and E.D. Williams, Phys. Rev. Lett. **58**, 2563 (1989).
[37] J. Wei, X.S. Wang, N.C. Bartelt, E.D. Williams, and R.T. Tung, J. Chem. Phys. **94**, 8384 (1991).
[38] G.E. Poirier, B.K. Hance, and J.M. White, J. Vac. Sci. Technol. B **10**, 6 (1992).
[39] J.K. Zuo, T. Zhang, J.F. Wendelken, and D.M. Zehner, Phys. Rev. B **63**, 033404 (2001).
[40] W. Weiss, K. Kasper, K.H. Herrmann, D. Schmeisser, and W. Gopel, Surf. Sci. **268**, 319 (1992).
[41] J.R. Heffelfinger, M.W. Bench, and C.B. Carter, Surf. Sci. **343**, L1161 (1995).
[42] J.R. Heffelfinger and C.B. Carter, Surf. Sci. **389**, 188 (1997).
[43] R.J. Phaneuf, N.C. Bartelt, E.D. Williams, W. Swiech, and E. Bauer, Phys. Rev. Lett. **67**, 2986 (1991).
[44] M. Horn-von Hoegen, F.J.M.Z. Heringdorf, D. Kahler, T. Schmidt, and E. Bauer, Thin Solid Films **336**, 16 (1998).
[45] G. Comsa, G. Mechtersheimer, and B. Poelsema, Surf. Sci. **119**, 159 (1982).
[46] C. Voss and N. Kruse, Surf. Sci. **409**, 252 (1998).
[47] V.K. Medvedev, Y. Suchorski, C. Voss, T. Visart de Bocarme, T. Bär, and N. Kruse, Langmuir **14**, 6151 (1998).
[48] K. Pelhos, T.E. Madey, and R. Blaszczyszyn, Surf. Sci. **426**, 61 (1999).
[49] H. Minoda and K. Yagi, Surf. Sci. **437**, L761 (1999).
[50] P. Pieranski, P. Sotta, D. Rohe, and M. Imperor-Clerc, Phys. Rev. Lett. **84**, 2409 (2000).
[51] V. Tsepelin, H. Alles, A. Babkin, J.P.H. Harme, R. Hochemsen, A.Ya. Parshin, and G. Tvalashvili, Phys. Rev. Lett. **86**, 1042 (2001).
[52] B.M. Ocko and S.G.J. Mochrie, Phys. Rev. B **38**, 7378 (1988).
[53] Q. Shen, J.P. Chang, G. Navrotski, and J. Blakely, Phys. Rev. Lett. **64**, 451 (1990).
[54] G.M. Watson, D. Gibbs, D.M. Zehner, M. Yoon, and S.G.J. Mochrie, Phys. Rev. Lett. **71**, 3166 (1993).
[55] A. Lied, H. Dosch, and J.H. Bilgram, Phys. Rev. Lett. **72**, 3554 (1994).
[56] M. Yoon, S.G.J. Mochrie, D.M. Zehner, G.M. Watson, and D. Gibbs, Surf. Sci. **338**, 225 (1995).
[57] G.M. Watson, D. Gibbs, S. Song, A.R. Sandy, S.G.J. Mochrie, and D.M. Zehner, Phys. Rev. B **52**, 12329 (1995).
[58] G.M. Watson, D. Gibbs, D.M. Zehner, M. Yoon, and S.G.J. Mochrie, Surf. Sci. **407**, 59 (1998).
[59] S. Song, S.G.J. Mochrie, and G.B. Stephenson, Phys. Rev. Lett. **74**, 5240 (1995).
[60] S. Song, M. Yoon, S.G.J. Mochrie, G.B. Stephenson, and S.T. Milner, Surf. Sci. **372**, 37 (1997).
[61] M. Yoon, S.G.J. Mochrie, M.W. Tate, S.M. Gruner, and E.F. Eikenberry, Surf. Sci. **411**, 70 (1998).
[62] A.J. Steinfort, P.M.L.O. Scholte, A. Ettema, F. Tuinstra, M. Nielsen, E. Landemark, D.-M. Smilgies, R. Fiedenhans'l, G. Falkenberg, L. Seehofer, and R.L. Johnson, Phys. Rev. Lett. **77**, 2009 (1996).
[63] M. Nielsen, D.-M. Smilgies, R. Fiedenhans'l, E. Landemark, G. Falkenberg, L. Lottermoser, L. Seehofer, and R.L. Johnson, Surf. Sci. **352–354**, 430 (1996).
[64] Z. Kovats, M. Rauscher, H. Metzger, J. Peisl, R. Paniago, H.-D. Pfannes, J. Schulze, I. Eisele, F. Boscherini, and S. Ferrer, Phys. Rev. B **62**, 8223 (2000).
[65] F.B. Rasmussen, J. Baker, M. Nielsen, R. Fiedenhans'l, and R.L. Johnson, Phys. Rev. Lett. **79**, 4413 (1997).
[66] E. Lundgren, J. Alvarez, X. Torrelles, K.F. Peters, H. Isern, and S. Ferrer, Phys. Rev. B **59**, 2431 (1999).
[67] G. Wulff, Z. Kristallogr. **34**, 449 (1901).
[68] H. P. Bonzel and K. Dueckers, in *Chemistry and Physics of Solid Surfaces VII*, edited by R. Vanselow and R. Howe (Springer-Verlag, Berlin, 1988), p. 429.
[69] E.D. Williams and N.C. Bartelt, Ultramicroscopy **31**, 36 (1989).
[70] J.W. Cahn, Acta Metall. **10**, 179 (1962).
[71] C. Herring, Phys. Rev. **82**, 87 (1951).
[72] J.W. Cahn and J.E. Hilliard, J. Chem. Phys. **31**, 688 (1959).
[73] J. Stewart and N. Goldenfeld, Phys. Rev. A **46**, 6505 (1992).
[74] M. Touzani and M. Wortis, Phys. Rev. B **36**, 3598 (1987).
[75] A. Shi and M. Wortis, Phys. Rev. B **37**, 7793 (1988).
[76] S. Wei and M.Y. Chou, Phys. Rev. B **50**, 4859 (1994).
[77] J.W.M. Frenken and P. Stoltze, Phys. Rev. Lett. **82**, 3500 (1999).
[78] W.W. Mullins, J. Appl. Phys. **30**, 77 (1959).
[79] W.W. Mullins, Philos. Mag. **6**, 1313 (1961).
[80] J.D. Shore, M. Holzer, and J.P. Sethna, Phys. Rev. B **46**, 11 376 (1992).
[81] F. Liu and H. Metiu, Phys. Rev. B **48**, 5808 (1993).
[82] D.G. Vlachos, L.D. Schmidt, and R. Aris, Phys. Rev. B **47**, 4896 (1993).
[83] J.D. Shore and D.J. Bukman, Phys. Rev. E **51**, 4196 (1995).
[84] H. Jeong and J.D. Weeks, Phys. Rev. B **57**, 3939 (1998).
[85] P.H. Fuoss and I.K. Robinson, Nucl. Instrum. Methods Phys. Res. B **222**, 171 (1984).
[86] I.K. Robinson, Phys. Rev. B **33**, 3830 (1986).
[87] D. A. Walko, Ph.D. thesis, University of Illinois at Urbana-Champaign, 2000.
[88] A. Munkholm and S. Brennan, J. Appl. Crystallogr. **32**, 143 (1999).
[89] M. Drechsler, Surf. Sci. **266**, 1 (1992).
[90] J.C. Boulliard and M.P. Sotto, Surf. Sci. **177**, 139 (1986).
[91] H. Jeong and J.D. Weeks, Surf. Sci. **432**, 101 (1999).
[92] E. Taglauer, S. Reiter, A. Liegl, and S. Schoemann, Nucl. In-

strum. Methods Phys. Res. B **118**, 456 (1996).
[93] L. Schwenger, R.L. Folkerts, and H.-J. Ernst, Phys. Rev. B **55**, 7406 (1997).
[94] I.K. Robinson, K.H. Whiteaker, and D.A. Walko, Physica B **221**, 70 (1996).
[95] R.H. Milne, Surf. Sci. **121**, 347 (1982).
[96] N. Cabrera, in *Symposium on Properties of Surfaces* (ASTM, Philadelphia, 1963), p. 24.